Transdermal delivery of interleukin-12 gene targeting dendritic cells enhances the anti-tumour effect of programmed cell death protein 1 monoclonal antibody

Huoyan Hong[1,#], Xiaoyun Wang[2,#], Xinran Song[1], Gomaa El Fawal[1,3], Kaili Wang[1], Di Jiang[1], Yifei Pei[1], Zhe Wang[1], Hongsheng Wang[1,]*

Key Words:

aPD-1; dendritic cells; ethosome; IL-12; transcutaneous immunization

ABSTRACT

Recent studies have suggested that the anti-tumour effect of the programmed cell death protein 1 monoclonal antibody (aPD-1) depends on the expression of interleukin-12 (IL-12) by dendritic cells (DCs). Since DCs are abundant in skin tissues, transdermal delivery of IL-12 targeting DCs may significantly improve the anti-tumour effect of aPD-1. In this study, a novel mannosylated chitosan (MC)-modified ethosome (Eth^{-MC}) was obtained through electrostatic adsorption. The Eth^{-MC} loaded with plasmid containing the IL-12 gene (p^{IL-12}@Eth^{-MC}) stimulated DCs to express mature-related molecular markers such as CD86, CD80, and major histocompatibility complex-II in a targeted manner. The p^{IL-12}@Eth^{-MC} was then mixed with polyvinyl pyrrolidone solution to make microspheres using the electrospray technique, and sprayed onto the surface of electrospun silk fibroin-polyvinyl alcohol nanofibres to obtain a PVP-p^{IL-12}@Eth^{-MC}/silk fibroin-polyvinyl alcohol composite nanofibrous patch (termed a transcutaneous immunization (TCI) patch). The TCI patch showed a good performance on transdermal drug release. Animal experiments on melanoma-bearing mice showed that topical application of the TCI patches promoted the expression of IL-12 and inhibited the growth of tumour. Furthermore, combined application of the TCI patch and aPD-1 showed a stronger anti-tumour effect than aPD-1 monotherapy. The combination therapy significantly promoted the expression of IL-12, interferon-γ and tumour necrosis factor-α, the infiltration of CD4$^+$ and CD8$^+$ T cells into tumour tissues, and thus promoted the apoptosis of tumour cells. The present study provides a convenient and non-invasive strategy for improving the efficacy of immune checkpoint inhibitor therapy. This study was approved by the Institutional Animal Care and Use Committee at Donghua University (approval No. DHUEC-NSFC-2020-11) on March 31, 2020.

Introduction

In recent years, immunotherapy has brought hope for the cure of malignant tumours. Programmed cell death-(ligand) 1 (PD-(L)1) is considered to be the most promising target for tumour immunotherapy, and the administration of anti-PD-(L)1 (aPD-(L)1) has achieved significant clinical efficacy in the treatment of lung cancer, advanced melanoma, bladder urothelial carcinoma, gastric cancer and other tumours.[1] However, more than half of patients are not sensitive to immune checkpoint blockers,[2, 3] and various combination therapies based on immune checkpoint blockers to enhance their efficacy are constantly being explored.[3-8] Recent studies have shown that the anti-tumour effect of aPD-1 requires the "authorization" of dendritic cells (DCs) to express interleukin-12 (IL-12): IL-12 stimulates T cells to release interferon-γ (IFN-γ), which can further activate the atypical nuclear factor-κB signalling pathway, activating DCs in an IL-12-dependent manner and enhancing the therapeutic effect of aPD-1.[1, 9, 10] Therefore, the effective activation of DCs to express IL-12 is critical in aPD-1 therapy.

DCs are the most powerful antigen-presenting cells *in vivo* and are abundant in the dermis and active epidermis of the skin.[11] The skin also contains other immune-active cells including Langerhans cells, macrophages, mast cells and T cells.[12, 13] Therefore, the skin is considered as the best site for immunization, thus giving rise to the concept of transcutaneous immunization (TCI).[11] Compared with traditional inoculation methods such as injection and oral administration, TCI has many advantages, including avoiding the

first pass effect of the liver and gastrointestinal irritation, being non-invasive, easy to use, and achieving good patient compliance.[14] However, the stratum corneum is a tight physical barrier of the skin, and it is difficult for macromolecular drugs such as antigens to be absorbed through the skin. Absorption requires the help of chemical penetration enhancers or nanocarriers. As chemical osmotic agents often cause adverse reactions such as skin irritation, lipid vesicles represented by ethosomes (Eths) have attracted much attention in recent years.[15] Eths are alcohol-containing liposomes with excellent flexibility and fluidity. The alcohol molecules contained in Eths enhance the ability of lipid vesicles to penetrate the stratum corneum, which give Eths good transdermal performance.[16, 17] Eths also have excellent drug-loading properties, including room temperature stability, high encapsulation efficiency and good biocompatibility.[15] Therefore, Eths are regarded as good carriers for drug delivery through transdermal route. We have reported recently that targeted delivery of antigen molecules to DCs via the transdermal route can trigger an effective immune response.[18] DCs express C-type lectin receptors on their surface, including DC-Sign, DEC-205, and mannose receptor.[18, 19] Liposomes modified with galactose or mannose groups have been shown to have the ability to target DCs and stimulate their maturation.[20-22] It is reasonable to assume that Eths modified with mannose groups on the surface would possess the ability to transdermally target DCs and could be a useful carrier for TCI.

IL-12 comprises two subunits, P35 and P40, which are produced by DCs and phagocytes after stimulation by microorganisms or cytokines.[23] IL-12 may be an ideal candidate for tumour immunotherapy due to its ability to activate innate and adaptive immunity.[24] IL-12 in tumours induces apoptosis of regulatory T cells and impairs memory $CD8^+$ T cells, leading to an influx of activated and lethal $CD4^+$ and $CD8^+$ T cells.[25] Although the anti-tumour effect of IL-12 has been confirmed by many studies, its clinical application is still difficult to popularize due to its short half-life and systemic toxicity. *IL-12* gene drugs may be a better choice to compensate for the short half-life of protein drugs.[26, 27] We hypothesized that transdermal delivery of the *IL-12* gene targeted to DCs by mannose-modified Eths could significantly improve the anti-tumour efficacy of aPD-1.

Electrospun nanofibres have unique advantages as sustained-release drug carriers due to their large specific surface area and high porosity.[28] Electrospun silk fibroin (SF) and polyvinyl alcohol (PVA) (SF-PVA) composite nanofibres have good skin affinity and mechanical properties, and are suitable for use as scaffolds for transdermal drug delivery. Polyvinylpyrrolidone (PVP) has good biocompatibility and is easily soluble in water.[29, 30] Electrostatic spray technology can be used to make the mixture of PVP and Eth into drug-loaded microspheres and attach them to nanofibrous mats, so as to obtain a convenient transdermal drug delivery patch. The high water solubility of PVP facilitates the rapid dissociation of drug-loaded Eths from the microspheres and their penetration into the skin.

In this study, a novel carrier for TCI was first fabricated by modifying hyaluronic acid (HA) and mannosylated chitosan (MC) successively on the surface of Eths via electrostatic adsorption and layer-by-layer self-assembly (the resulting product was named Eth^{-MC}). The Eth^{-MC} loaded with plasmid containing the *IL-12* gene (p^{IL-12}@Eth^{-MC}) was then mixed with PVP solution to make microspheres and sprayed onto the electrospun SF-PVA nanofibres by electrospraying to obtain a PVP-p^{IL-12}@Eth^{-MC}/SF-PVA nanofibrous patch (named a TCI patch). The ability of p^{IL-12}@Eth^{-MC} to target DCs to induce their maturation was verified by *in vitro* phagocytosis experiments, and melanoma-bearing mice were used as a model to investigate the anti-tumour activity of the as-prepared TCI patch and to ascertain whether it can enhance the anti-tumour effect of aPD-1.

Methods

Synthesis of mannosylated chitosan

MC was synthesized by a method previously reported.[31] In short, chitosan (Sigma-Aldrich, St. Louis, MO, USA) was dissolved in 1% acetic acid to prepare a 2.0 mg/mL solution. Aqueous solutions of D-mannose (20 mM; Sigma-Aldrich) and NaBH(OAc)$_3$ (20 mM; Yien Biotechnology Co., Ltd., Shanghai, China) were also prepared, then equal volumes of the three solutions were evenly mixed by slowly stirring at room temperature for 48 hours, dialyzed in a dialysis bag (MWCO 12–14 kDa, Beijing Jingke Hongda Biotechnology Co. Ltd., Beijing, China) against deionized water for 72 hours, and freeze-dried to obtain the MC.

Preparation of mannosylated chitosan-modified ethosomes

Eths were prepared following a previously-described method.[14] Briefly, 10 mg cholesterol (Sigma-Aldrich), 100 mg egg yolk lecithin (Sigma-Aldrich) and 4 mg octadecylamine were dissolved in 5 mL absolute ethanol at room temperature, and then rotary evaporated at 40°C to obtain a lipid film. Subsequently, 10 mL 30% ethanol containing 0 or 40 µg/mL *IL-12* gene expression plasmid (p^{IL-12}; Hunan Fenghui Biotechnology Co., Ltd., Changsha, China) was added to rehydrate the film by agitating for 30 minutes at room temperature. A probe ultrasonic instrument (JY92-II, Ningbo Kechuang Biotechnology Co., Ltd., Ningbo, China) was used to obtain homogenous suspension of cationic Eths loaded with p^{IL-12}, and the non-encapsulated free drugs were removed by centrifugation at 12,787 × *g* for 10 minutes. Then, filtering the solutions multiple times using a 220 nm microporous membrane, Eths (Eth or p^{IL-12}@Eth) with uniform particle size was obtain. An equal volume of 1 mg/mL HA aqueous solution (Sigma-Aldrich) was added into the Eth solution and slowly stirred at room temperature for 2 hours to obtain HA-coated Eths (Eth^{-HA} or p^{IL-12}@Eth^{-HA}), then centrifuged at

1 Shanghai Engineering Research Centre of Nano-Biomaterials and Regenerative Medicine, Key Laboratory of Science & Technology of Eco-Textile (Ministry of Education), College of Chemistry, Chemical Engineering and Biotechnology, Donghua University, Shanghai, China; 2 Department of Obstetrics & Gynaecology, Shanghai First People's Hospital Affiliated to Shanghai Jiao Tong University, Shanghai, China; 3 Department of Polymer Materials Research, Advanced Technology and New Materials Research Institute, Scientific Research and Technological Applications City (SRTA-City), New Borg El-Arab City, Alexandria, Egypt

12,787 × *g* for 10 minutes to remove free HA. Subsequently, an equal volume of Eth^-HA^ and 1% (w/v) MC acetic acid solution (pH = 4.0) were mixed and stirred at room temperature for 2 hours. After removing free MC by centrifugation at 12,787 × *g* for 10 minutes, MC-coated Eths (Eth^-MC^ or p^IL-12^@Eth^-MC^) were obtained. Next, 0.2 mL of 1,1′-dioctadecyl-3,3,3′,3′-tetramethylindocarbocyanine perchlorate (DiI; Sigma-Aldrich) was added to 10 mL of Eth solution, stirred for 30 minutes and dialyzed against deionized water for 3 days (changing the water three times a day) to obtain DiI-labelled Eths. Free DiI and DiI aggregates were removed through centrifugation at 12,787 × *g* for 10 minutes. The Eths were characterized by transmission electron microscopy (JEM-2100, Jeol Ltd., Tokyo, Japan), laser particle analysis (BI-200SM, Brookhaven Instruments, Holtsville, NY, USA) as well as measuring zeta potential (Malvern Instruments, Malvern, UK).

Gel retardation assay

The optimum octadecylamine:pIL-12 (N/P) ratio of cationic Eths loaded with DNA was investigated by the gel block method[32] to explore the ability of the carrier to condense DNA. The plasmid-loaded Eths were prepared with N/P ratios of 1:5, 1:10, 1:15 and 1:20. After mixing with loading buffer, the plasmid-loaded Eths were placed into a sample well of a 1% agarose gel, and electrophoresed in Tris/borate/ethylene diamine tetraacetic acid buffer at 90 V for 25 minutes, and then photographed with a gel imager (FR-980B, Shanghai Furi Technology Co., Ltd., Shanghai, China).

Cytotoxicity assay

Viability of the Eth-treated cells was assessed by Cell Counting Kit-8 (CCK-8) and live/dead staining assays. DC2.4 cells (Hunan Fenghui Biotechnology Co., Ltd.) were seeded into a 24-well plate at a cell density of 1.5×10^4/well and cultured at 37°C in a humidified incubator with 5% CO_2 using RPMI 1640 medium (Gibco, Carlsbad, CA, USA) supplemented with 1% (v/v) penicillin/streptomycin and 10% (v/v) fetal bovine serum (Gibco). Medium was discarded after culturing for 24 hours, 1 mL of fresh medium containing different concentrations of the carrier materials was added (the wells without carriers were used as controls) and cultures were returned to the incubator for a further 24 hours.

For CCK-8 assay, medium was removed and the cell layer was washed with sterile phosphate-buffered saline (PBS) three times, then 400 μL fresh RPMI 1640 medium (without fetal bovine serum) containing 40 μL CCK-8 reagent (Biyuntian Biotechnology Co., Ltd., Shanghai, China) was added to each well, and the plate was incubated at 37°C in the dark for 1 hour, after which 100 μL of each sample was transferred to a 96-well plate. A microplate reader (Multiskan MK3, Thermo Fisher Scientific, Waltham, MA, USA) was used to measure the absorbance at 450 nm. The following formula was used to calculate the cell survival rate: Cell viability (%) = (At – Ab)/(Ac – Ab) × 100 (At: absorbance of the tested samples; Ab: absorbance of the blank wells containing culture medium and CCK-8 solution but without cells; Ac: absorbance of the controls).

For live/dead staining assay, calcium-AM/propidium iodide double staining was used to evaluate the growth state of the cells co-incubated with Eth-MC at different concentrations. After co-incubation for 24 hours, the medium was removed and the cells were washed three times with PBS. Then, 200 μL of 5 μM calcein-AM (Biyuntian Biotechnology Co., Ltd.) and 10 μM propidium iodide (Biyuntian Biotechnology Co., Ltd.) were added to each well and the plate was incubated at 37°C in the dark for 15 minutes. Cell morphology was finally observed using an inverted fluorescence microscope (DMi 8, Leica Microsystems Ltd., Wetzlar, Germany).

Targeted induction of dendritic cells by Eth^-MC^ *in vitro*
Phagocytosis of Eth^-MC^ by dendritic cells

DC2.4 cells (2×10^5/well) were seeded evenly onto a confocal culture dish and treated with 30 μL DiI-labelled Eths (30 μg/mL) at 37°C for 2 hours in the dark, cells treated with the same volume of PBS were used as control. Then, cells were washed three times with PBS, fixed for 30 minutes using 4% paraformaldehyde and stained with 4,6-diamino-2-phenylindole dihydrochloride (Sigma-Aldrich) for 10 minutes. After washing again with PBS three times, samples were observed using a confocal laser scanning microscope (ZEISS LSM 700, Zeiss, Jena, Germany). The fluorescence intensity of different samples was compared and analysed using ImageJ 1.44 software (National Institutes of Health, Bethesda, MD, USA).

Transfection of dendritic cells and L929 with p^IL-12^-loaded ethosomes

The mouse skin fibroblasts L929 were provided by the Institute of Biochemistry and Cell Biology, Chinese Academy of Sciences (Shanghai, China). L929 cells (cultured with high-glucose Dulbecco's modified Eagle medium (Gibco) supplemented with 10% (v/v) fetal bovine serum and 1% (v/v) penicillin/streptomycin) and DC2.4 cells were seeded into a 6-well plate at 2×10^5/well and incubated at 37°C in 5% CO_2. When the cells reached 80% confluence, medium was refreshed and Eths loaded with 2.5 μg p^IL-12^ were added and incubated for 24 hours. After that, total RNA was extracted from the cells and reverse transcribed into complementary DNA using a kit (NovoProtein Technology Co., Ltd.). The mRNA expression of *IL-12a* and *IL-12b* was then analysed by real time fluorescence quantitative polymerase chain reaction on a polymerase chain reaction machine (7500, Applied Biosystems Inc., Foster City, CA, USA), under the following conditions: denaturation at 95°C for 2 minutes, followed by 40 cycles of 95°C for 15 seconds and 62°C for 32 seconds. The housekeeping gene *β-actin* was used as an internal reference control and the relative expression level of *IL-12* was calculated by the $2^{-\Delta\Delta Ct}$ method (**Table 1**).[33]

Induction of dendritic cell maturation by p^IL-12^-loaded ethosomes

DC2.4 cells were seeded into a 6-well plate at 1.5×10^5/well, and co-cultured with 30 μL of unmodified Eths or p^IL-12^-loaded Eths for 24 hours. Cells treated with lipopolysaccharide (100 ng/mL; Sigma-Aldrich) or PBS were used as the positive or negative control, respectively. Cells were harvested and centrifuged at 250 × *g* for 5 minutes, washed with PBS for three times, then incubated with phycoerythrin-labelled goat anti-

Table 1. Primer sequences for real-time fluorescence quantitative polymerase chain reaction

Gene	Sequence (5′–3′)
β-Actin	Forward: GGC TGT ATT CCC CTC CAT CG
	Reverse: CCA GTT GGT AAC AAT GCC ATG T
IL-12a	Forward: TCC AGC AGC TCC TCT CAG TG
	Reverse: ACT GGC TAA GAC ACC TGG CA
IL-12b	Forward: GGC TGG ACT GCA TGA TAG CG
	Reverse: GCC AGG ATG TCT CTG CTC CT

Note: IL-12: interleukin-12.

mouse CD80, major histocompatibility complex-II and CD86 monoclonal antibodies (PeproTech, Rocky Hill, NJ, USA) at 4°C for 30 minutes. After again washing with PBS three times, the samples were analysed by flow cytometry using a FACSCalibur machine (Becton Dickinson, Franklin Lakes, NJ, USA).

Preparation and characterization of the transcutaneous immunization patch

Preparation of silk fibroin and polyvinyl alcohol nanofibres

SF was prepared according to the previously-described method.[14] Briefly, the mulberry silkworm cocoons (Huzhou Silk Company, Huzhou, China) were degummed three times with 0.5% (w/v) Na_2CO_3 solution at 100°C for 30 minutes, and then washed with warm water. After drying, the degummed silk (SF) was dissolved in 9.3 M lithium bromide (Sigma-Aldrich) at 60°C for 1 hour to obtain a uniform solution. After three days of dialysis with a dialysis bag (molecular weight cut-off = 14,000 kDa) against deionized water at room temperature, the SF solution was filtered and lyophilized to obtain regenerated SF sponges.

Aqueous solutions of 8% PVA (Sigma-Aldrich) and 6% SF were prepared, mixed together at a volume ratio of 5:2 (PVA:SF) and stirred for 12 hours at room temperature to obtain stable spinning solutions, which were then electrospun at a voltage of 15 kV, an extrusion rate of 1 mL/h and a receiving distance of 15 cm. The resulting product was placed in a vacuum dryer (DZF-6020, Yiheng Technology Co., Ltd., Shanghai, China) for drying and storage before use.

Preparation of microsphere-loaded silk fibroin and polyvinyl alcohol nanofibrous patches

First, 1 g PVP was dissolved in 6 mL of 60% ethanol solution, then blended with 4 mL p^{IL-12}@Eth^{-MC} to obtain a well-mixed solution by gentle stirring at room temperature for 2 hours. Next, the mixed solution was taken into a syringe and microspheres (PVP-p^{IL-12}@Eth^{-MC}) were sprayed onto the surface of the SF-PVA nanofibres. The conditions set for electrospraying were as follows: voltage 18 kV, receiving distance 15 cm, extrusion rate 0.8 mL/h, temperature 40°C, humidity 8%. The obtained product was a PVP-p^{IL-12}@Eth^{-MC}/SF-PVA composite nanofibrous patch, which is referred to as a TCI patch in this study. The TCI patches were dried and stored in a vacuum dryer before use.

The surface morphology of the TCI patch was characterized using a scanning electron microscope (TM-1000, Hitachi, Tokyo, Japan) and the distribution of DiI-labelled Eths in the patch was observed with a fluorescence microscope (DMi 8).

In vitro transdermal test

Mouse skin was prepared according to a previously-described method[14] and stored at −20°C until further use. A Franz diffusion pool was used to assess the transdermal performance of the TCI patches according to a published method.[14] Briefly, the prepared skin (with the surface of the stratum corneum facing upwards) was sandwiched between the receiving pool and the donor pool of the diffusion cell system, and a patch containing 4 μg of p^{IL-12} labelled with Hoechst 33342 (Biyuntian Biotechnology Co., Ltd.) was attached tightly to the skin surface. The receiving pool was filled with PBS (pH = 7.4) and stirred continuously at 350 r/min while maintaining at 33°C in a water bath. At appropriate time intervals (0.5, 1, 2, 4, 6, 8, 10, 12, and 24 hours), 2 mL of receiving solution was removed from the sampling port and added to an equal volume of fresh buffer. Under 354 nm excitation and 458 nm emission wavelengths, the absorbance value of the receiving solution samples were determined using an ultraviolet spectrophotometer (UV1100, Shanghai Mapada Instrument Co., Ltd., Shanghai, China). The cumulative release amount of the plasmid was then calculated according to the following formula:

$$Q = \frac{VCn + \sum_{i=1}^{n-1} CiVi}{Q'} \times 100\%$$

where Q is the cumulative amount of drug released, Q' is the actual amount of drug contained in the Eths, V is the volume of the diffusion pool, Ci is the drug concentration at i sampling time, and Vi is the volume at i sampling time.

Data were also expressed as the cumulative drug permeation per unit of skin surface area, Qt/S (S = 1.13 cm^2). The steady-state fluxes ($Jss_{(2-24h)}$) were calculated at steady state between 2 and 24 hours as shown in the following formula:[34] $Jss_{(2-24h)} = \Delta Qt/\Delta t \times s$. where ΔQt is the cumulative drug permeation within a certain period (Δt).

The p^{IL-12}@Eth^{-MC} treated skin was removed from the Franz diffusion cells at different time points (2, 4, 8, and 12 hours) embedded in paraffin and sequentially sectioned. The distribution of fluorescence in the skin was observed using fluorescence microscopy (DMi 8) and the fluorescence intensity of different samples was compared and analysed using ImageJ 1.44 software.

Animal experiments

Five-week-old C57BL/6 male mice (Shanghai SLAC Laboratory Animal Co., Ltd., Shanghai, China; license No. SCXK (Hu) 2012-0002) were maintained in a 12-hour light/

dark cycle with free access to food and water (specific pathogen-free environment). All animal experiments were performed according to the guidelines approved by the Institutional Animal Care and Use Committee of Donghua University (approval No. DHUEC-NSFC-2020-11, on March 31, 2020).

Mice were inoculated with B16-F10 cells (a mouse melanoma cell line, provided by the Institute of Biochemistry and Cell Biology, Chinese Academy of Sciences, 1×10^6/mouse) on the side of the thighs and randomly divided into four groups, each with 11 mice: control (not receiving any treatment), TCI monotherapy, aPD-1 monotherapy, and combination therapy (TCI + aPD-1). The TCI patches (each contained 4 g p$^{\text{IL-12}}$) were applied to the hairless dorsal skin of the mice. Before application, the skin was moistened with water to make the patch adhere closely to the skin, and then fixed in position with medical tape. The aPD-1 was administered by intraperitoneal injection (20 µg/mouse/time). Tumour length (L) and width (W) were measured every 2–3 days, and tumour volume (V) was calculated according to the following formula: V = (L × W^2)/2. A mouse with a tumour volume exceeding 2000 mm^3 was considered dead. Mouse body weights were also recorded every 2–3 days. Blood was collected on days 10, 17, and 24 in each group, and serum levels of IFN-γ, IL-12, and tumour necrosis factor-α (TNF-α) were determined by enzyme-linked immunosorbent assay according to the manufacturer's protocol (PeproTech). Briefly, the microtiter plates were coated with purified antibodies (anti-mouse IFN-γ, IL-12 or TNF-α) to make solid phase antibodies, and IFN-γ (IL-12 or TNF-α) were added. Then, horseradish peroxidase-labeled secondary antibodies were added to form antibody-antigen-enzyme-labeled antibody complex. After thorough washing, 3,3′,5,5′-tetramethylbenzidine was added for color rendering. The optical density at 450 nm was measured with a microplate reader (Multiskan MK3), and the concentration of IFN-γ (IL-12 or TNF-α) was calculated according to the standard curve. On day 24, the mice were sacrificed by cervical dislocation, and tumours, hearts, livers, spleens, lungs and kidneys were all removed and fixed in 4% paraformaldehyde solution. The tumour tissues were stained with terminal deoxynucleotidyl transferase-mediated dUTP nick-end labelling and immunohistochemical staining of anti-CD4 and CD8. For terminal deoxynucleotidyl transferase-mediated dUTP nick-end labelling, proteinase K was add to cover the tissue slices and incubated at 37°C for 25 minutes. Washing with PBS (pH 7.4) for 10 minutes, the samples were incubated with membrane breaking solution at room temperature. Washing and dry, the slices were incubated with terminal deoxynucleotidyl transferase, FITC-labeled dUTP and buffer (mix at 1:5:50 ratio) at 37°C for 2 hours. The samples were washed with PBS, covered with anti-fade mounting medium, observed under fluorescence microscope (DMi 8). For immunohistochemical staining of anti-CD4 and CD8, the tissue slides were immersed in ethylenediaminetetraacetic acid antigen retrieval buffer (pH 8.0) and maintained at a sub-boiling temperature for 15 minutes. Washing and eliminating obvious liquid, the tissue was blocked with 3% bovine serum albumin for 30 minutes. Throwing away the blocking solution slightly, the tissue was incubated with primary antibodies overnight at 4°C, and

placed in a wet box containing a little water. After washing slides three times with PBS and throwing away liquid slightly, the tissue was incubated with secondary antibodies at room temperature for 50 minutes in dark. Washing three times, the sample was incubated with 4,6-diamino-2-phenylindole dihydrochloride solution at room temperature for 10 minutes in dark. After washed three times with PBS, the sample was incubated with spontaneous fluorescence quenching reagent for 5 minutes. The samples were washed in running tap water for 10 minutes, covered with anti-fade mounting medium and observed by fluorescent microscopy (DMi 8). At the same time, paraffin sections of tumour and viscera were prepared, stained with hematoxylin–eosin, examined and photographed under a microscope (DMi 8).

Statistical analysis

All experiments were carried out at least three times and data are reported as mean ± standard deviation (SD). OriginPro 8.0 (OriginLab Corporation, Northampton, MA, USA) was used to perform one-way analysis of variance with Tukey's *post hoc* test for statistical analysis. A *P* value of < 0.05 was considered significant.

Results
Characterization of Eth$^{\text{-MC}}$
In the mannose coupling reaction, the aldehyde group of ring opening mannose reacted with the free amino group of chitosan to form a Schiff's base (R-CH=N-R bond), which was confirmed by the N-H bending of secondary amine at 1558.54 cm^{-1} and the C-N stretching vibration peak at 1410.01 cm^{-1} [31] (**Figure 1A**). The variation of the characteristic peaks from 3304.17 cm^{-1} to 3383.26 cm^{-1} further confirmed the above conclusion. In addition, the extensive and strong OH stretch at 3383.26 cm^{-1} and the strong CO stretch at 1076.32 cm^{-1} in the spectrum of MC proved that there were a large number of hydroxyl groups (from mannose), indicating that mannose groups were successfully attached to chitosan.[35] In the spectrum of HA, the characteristic peaks at 1609.43 cm^{-1} and 1032.34 cm^{-1} are strong amide and C-O-C chemical bonds, respectively.[36] MC has its characteristic peaks at 1595.18 cm^{-1} and 1410.01 cm^{-1}.[31] For Eth, the characteristic peaks at 2920.80 cm^{-1} and 2851.50 cm^{-1} represented the stretching vibration of the C-H bond and the H-C-H symmetrical stretching peak, respectively.[37] Compared with the Eth, the absorption peak intensity at 1032.34 cm^{-1} in the spectrum of Eth$^{\text{-HA}}$ was significantly enhanced, indicating that HA was successfully adsorbed onto the Eth. In the spectrum of Eth$^{\text{-MC}}$, the intensity of the absorption peak at 1595.18 cm^{-1} and 1410.01 cm^{-1} was significantly enhanced, indicating that MC was successfully adsorbed onto Eth$^{\text{-HA}}$.

Figure 1B shows the particle size and electric potential of the Eths. Since positively-charged octadecamine was used in the preparation of Eths, the obtained Eths were positively charged with a potential of +21.3 mV. HA is negatively charged and can be adsorbed onto the surface of cationic Eths through electrostatic interaction to obtain Eth$^{\text{-HA}}$ with a potential of −18.26 mV. Positively-charged MC was then further adsorbed

onto the surface of Eth-HA to obtain positively-charged Eth-MC with a potential of +25.90 mV. This modification also showed a significant effect on the particle size of Eths. The size of Eth-HA was almost doubled compared with the bare Eth, which may be due to the hydration of HA.[16] The particle size of Eth-MC was significantly reduced compared with Eth-HA, which might be due to the compact structure between HA and MC caused by the attraction of charges.[14] The morphology of Eths showed a multi-layer cystic spherical structure (**Figure 1C**). The results of agarose gel electrophoresis showed that no bright bands were

visible in the sample well when the ratio of octadecylamine to plasmid was higher than 1:10, i.e. p^{IL-12} was physically encapsulated within the inner cavity of the Eth-MC (**Figure 1D**). When the ratio was less than 1:15, some of the DNA that could not be completely enclosed was electrostatically adsorbed onto the surface of the positively-charged Eth-MC, causing a bright band to appear in the sample well. In order to allow the Eth-MC to completely encapsulate as much DNA as possible in its inner cavity through physical encapsulation, a 1:10 N/P ratio was used to load p^{IL-12} in subsequent experiments.
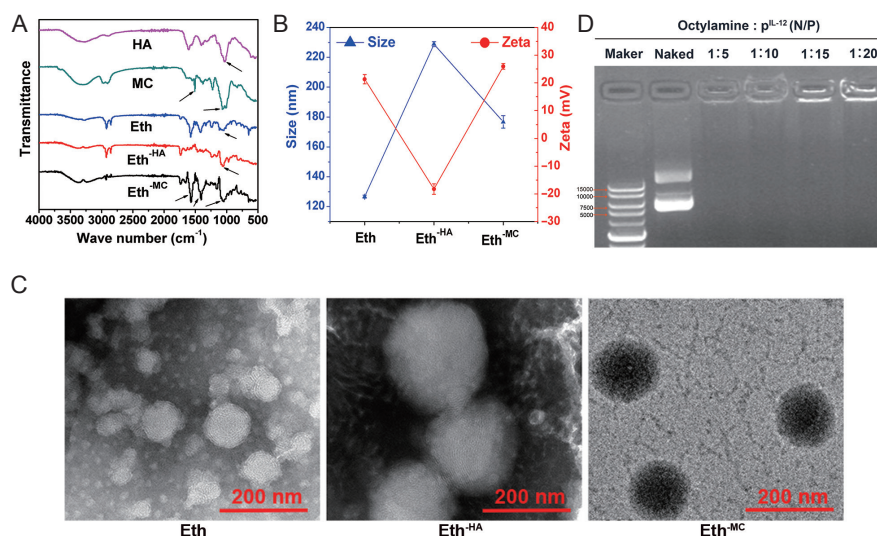

Figure 1. Characterization of Eths. (A) Infrared spectra of the materials. Arrows indicate the characteristic peaks. (B) Particle size and electric potential. Data are expressed as mean ± SD. The experiments were repeated by three times. (C) Transmission electron microscopy images of Eths. The adsorption of HA made the particle size of Eth increase significantly while the potential greatly reduced. When MC is further adsorbed on the surface of HA, the particle size decreases but is still larger than bare Eth, and the potential increased slightly. Scale bars: 200 nm. (D) Image of agarose gel electrophoresis at different octadecylamine:p^{IL-12} ratios. Eth: ethosome; HA: hyaluronic acid; MC: mannosylated chitosan; p^{IL-12}: plasmid containing *IL-12* gene.

Cytotoxicity of the ethosomes

CCK-8 assay was used to determine the cytotoxicity of the Eths. As shown in **Figure 2A**, the viability of DCs was not significantly reduced when the concentration of carriers did not exceed 10 μg/mL. The Eth-HA showed excellent cytocompatibility, which might be attributable to HA being negatively charged. Among the three carriers, Eth-MC showed the worst cytocompatibility, which is likely to be due to its higher potential. At concentrations of no more than 30 μg/mL, Eth-MC showed good cytocompatibility (cell viability was more than 80% of the control). When the concentration reached 40 μg/mL, Eth-MC exhibited obvious cytotoxicity. The results of live and dead cell staining showed a similar trend with that of CCK-8 (**Figure 2B**). Based on these results, the Eth-MC concentration was set to 30 μg/mL in subsequent studies, considering a balance between cytotoxicity and drug dosage.

Dendritic cell-targeted performance of Eth-MC

To evaluate the targeting performance of the carriers, DCs were treated with DiI- (red fluorescent dye) labelled carriers. The phagocytosis of the carriers by DCs was observed by confocal laser scanning microscopy. As shown in **Figure 3A & B**, the intensity of red fluorescence in the Eth-MC treated cells was significantly higher than that of the Eth and Eth-HA

cells, indicating that DCs have a selective preference for the phagocytosis of Eth-MC, that is, Eth-MC has good ability to target DCs. Eth-treated cells showed weak red fluorescence, indicating that Eth can be taken up by DCs in a non-targeted manner. Eth-HA was least engulfed by DCs, which may be due to its negative surface charge and larger particle size. The expression level of IL-12 in DC2.4 cells after transfection was significantly higher than that of L929 cells, and Eth-MC induced a much higher expression than Eth-HA or bare Eth did (**Figure 3C**). These data indicated that Eth-MC has the ability to target DCs.

p^{IL-12}@Eth-MC induces dendritic cells to mature

To investigate whether p^{IL-12}@Eth-MC can induce DC maturation, flow cytometry was used to detect the expression of CD80, CD86 and major histocompatibility complex-II which are markers related to the maturation of DCs. After co-incubation for 24 hours, the expression levels of the above markers in the groups with p^{IL-12} loaded carriers were much higher than those with lipopolysaccharide (used as positive control) or empty carriers (**Figure 4A & B**). In addition, the p^{IL-12}@Eth-MC induced significantly higher levels than the p^{IL-12}@Eth, indicating that p^{IL-12}@Eth-MC can effectively stimulate DC maturation.
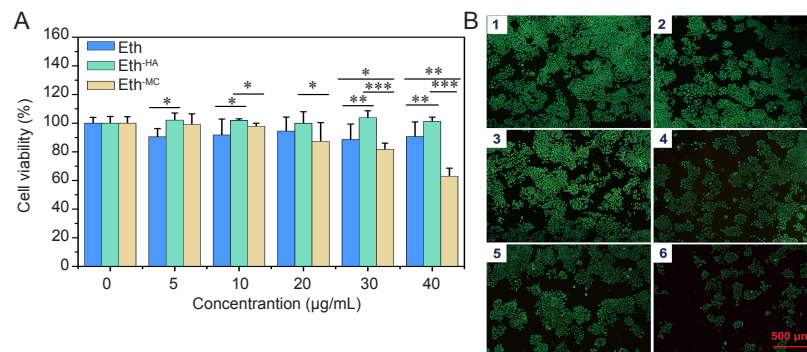
Figure 2. Cytotoxicity of Eths with different modifications as evaluated by Cell Counting Kit-8. (A) Cell viability. Data are expressed as mean ± SD. The experiments were repeated by three times. *$P < 0.05$, **$P < 0.01$, ***$P < 0.001$ (one-way analysis of variance followed with Tukey's *post hoc* test). (B) Live and dead staining of Eth^{-MC}-treated cells. There was no significant difference in cell morphology among different groups, but cell proliferation was inhibited to a certain extent when the concentration of Eth^{-MC} is higher than 30 μg/mL. B1–6: 0, 5, 10, 20, 30, and 40 μg/mL. The green fluorescence indicates live cells. Scale bars: 500 μm. Eth: ethosome; HA: hyaluronic acid; MC: mannosylated chitosan.
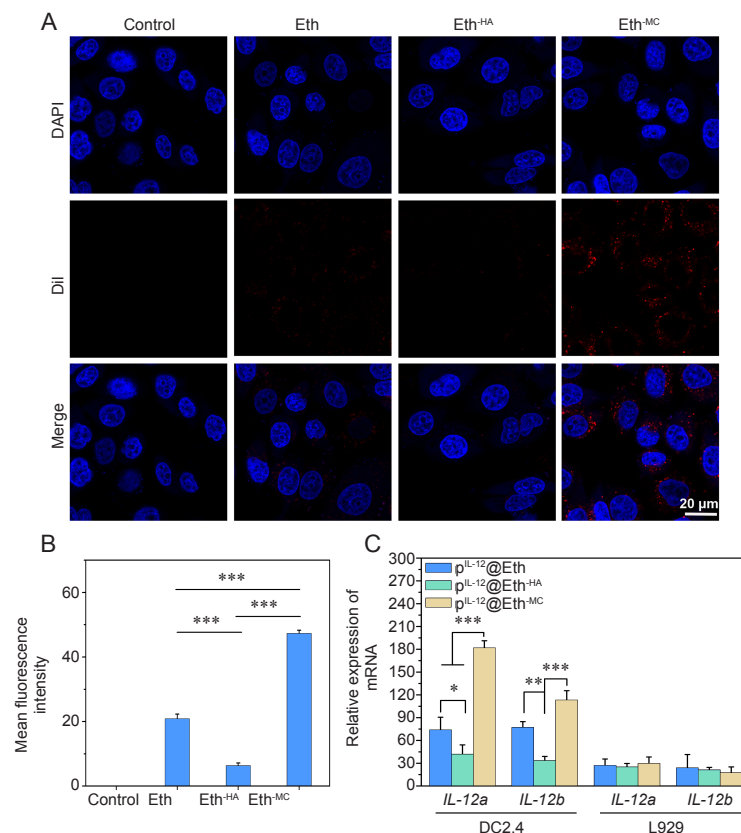
Figure 3. Performance of Eths targeting dendritic cells. (A) Confocal laser scanning microscopy images of dendritic cells phagocytosing DiI (red)-labelled Eths. The phagocytosis efficiency of Eth^{-MC} was significantly higher than that of others. Scale bars: 20 μm. (B) Fluorescent intensity analysis of A. (C) Relative mRNA expression of *IL-12* in different cells transfected with p^{IL-12}@Eths detected by real-time polymerase chain reaction. Data are expressed as mean ± SD. The experiments were repeated by three times. *$P < 0.05$, **$P < 0.01$, ***$P < 0.001$ (one-way analysis of variance followed with Tukey's *post hoc* test). DAPI: 4,6-diamino-2-phenylindole dihydrochloride; DiI: 1,1′-dioctadecyl-3,3,3′,3′-tetramethylindocarbocyanine perchlorate; Eth: ethosome; HA: hyaluronic acid; IL-12: interleukin-12; MC: mannosylated chitosan; p^{IL-12}: plasmid containing *IL-12* gene.

Characterization of the transcutaneous immunization patch
Morphology
SF-PVA composite nanofibrous mats with high porosity were first prepared by electrospinning, and the average fibre diameter was 449 ± 107 nm (**Figure 5A**). Then, the PVP-Eth^{-MC}

microspheres (**Figure 5B1**) were sprayed onto the SF-PVA composite nanofibrous mats using electrospraying technology to obtain a TCI patch as shown in **Figure 5C1**. The average diameter of the microspheres was 658 ± 175 nm (**Figure 5B2**), and they were evenly distributed on the surface of SF-PVA composite nanofibrous mats (**Figure 5C1**). The existence of Eth^{-MC} on

the TCI patch was confirmed by fluorescence microscopy, as shown in **Figure 5C2**, where Eth^{-MC} was labelled with DiI (a red fluorescent dye). The high specific surface area and high porosity of the composite nanofibrous mats are conducive to close contact between the drug-loaded microspheres and skin cells, thereby contributing to the transdermal drug release of Eth^{-MC}.
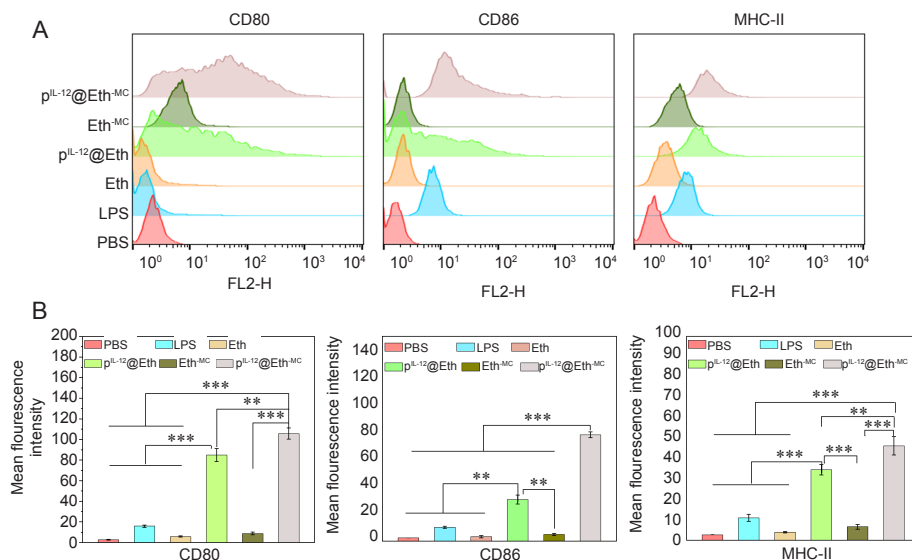

Figure 4. *IL-12* gene-loaded Eths stimulate DCs expression of CD80, CD86 and MHC-II. (A) Flow cytometry histograms. (B) Quantitative analysis of CD80, CD86 and MHC-II. Data are expressed as mean ± SD. The experiments were repeated by three times. **$P < 0.01$, ***$P < 0.001$ (one-way analysis of variance followed with Tukey's *post hoc* test). Eth: ethosome; HA: hyaluronic acid; IL-12: interleukin-12; LPS: lipopolysaccharide; MC: mannosylated chitosan; MHC-II: major histocompatibility complex-II; PBS: phosphate-buffered saline; p^{IL-12}: plasmid containing *IL-12* gene.
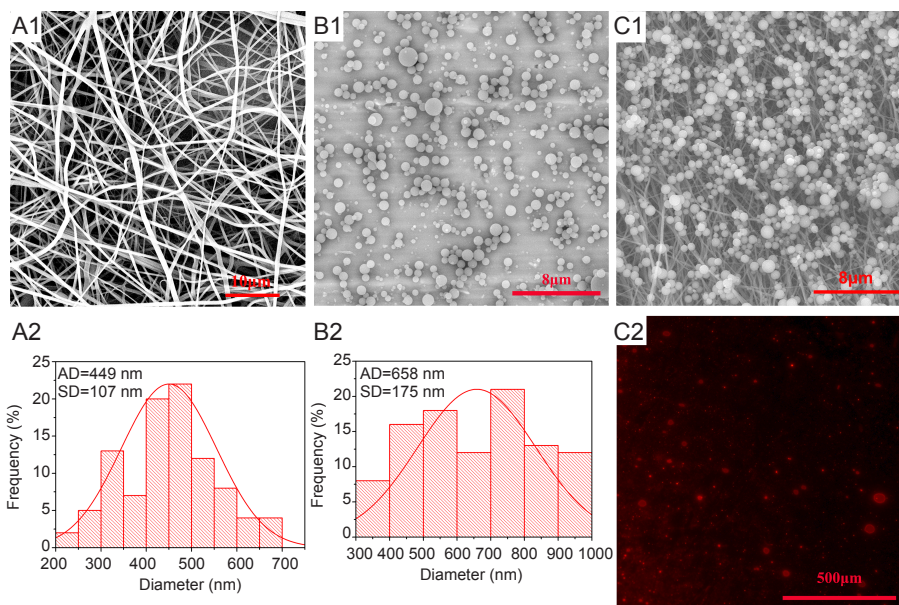

Figure 5. Morphology of SF-PVA nanofibrous mats (A1), microspheres (B1) and TCI patch (C1). (A2) Distribution of diameters in A1. (B2) Distribution of diameters in B1. (C2) Fluorescence micrograph of TCI patch. Red represents DiI-labeled Eth^{-MC}. Scale bars: 10 μm in A1, 8 μm in B1 and C1, 500 μm in C2. AD: average diameter; Eth^{-MC}: mannosylated chitosan-modified ethosome; PVA: polyvinyl alcohol; SF: silk fibroin; TCI: transcutaneous immunization.

Transdermal performance of the transcutaneous immunization patch

The p^{IL-12} was labelled with Hoechst 33342 and the transdermal performance of the TCI patches was evaluated using a Franz diffusion pool *in vitro*. As shown in **Figure 6A**, the cumulative transdermal drug release over 36 hours for p^{IL-12}@Eth- or p^{IL-12}@Eth^{-MC}-loaded TCI patches were 27.3% and 26%, respectively. The data of steady-state flux showed a similar trend to that of the cumulative release, at 0.030 μg/h/cm^2 for p^{IL-12}@Eth and 0.029 μg/h/cm^2 for p^{IL-12}@Eth^{-MC} (**Figure 6B**). These results suggested that the transdermal performance of the Eth can be slightly affected by modification with HA and MC, which may be due to the increased particle size after modification. **Figure 6C** & **D**

shows the permeation and distribution of the DiI-labelled Eth[-MC] and Hoechst 33342-labelled p[IL-12] in skin tissue after the transdermal application of the TCI patches for different times. The carriers and drugs were mostly distributed in the stratum corneum within 2 hours. When the administration

time was extended to more than 4 hours, the carrier and drugs completely penetrated into the dermis layer of the skin. These results indicate that the as-prepared TCI patch can effectively deliver plasmid DNA (molecular weight greater than 1×10^6) through the transdermal route.
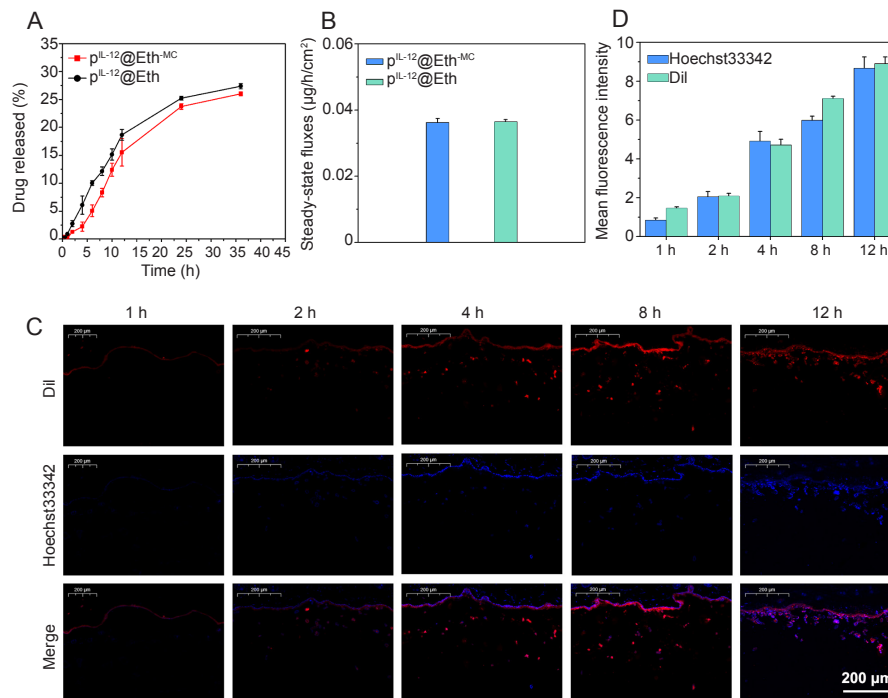
Figure 6. (A, B) *In vitro* cumulative transdermal drug release curve (A) and its Steady-state release flux (B). (C, D) Fluorescence images of skin sections (C) and their fluorescent intensity analysis (D) after transdermal administration with p[IL-12]@Eth[-MC]. The amount of Eth and DNA that penetrate into the skin tissue increases with time. Scale bar: 200 μm. Data are expressed as mean ± SD. The experiments were repeated by three times. DiI: 1,1′-dioctadecyl-3,3,3′,3′-tetramethylindocarbocyanine perchlorate; Eth: ethosome; IL-12: interleukin-12; MC: mannosylated chitosan; p[IL-12]: plasmid containing *IL-12* gene.

Anti-tumour effect of combination therapy with a transcutaneous immunization patch and aPD-1
Expression levels of interleukin-12, interferon-γ and tumour necrosis factor-α under different treatments
After treatment with the TCI patch and/or aPD-1, blood samples were taken from the eyes at different time points, and secretion levels of IL-12, IFN-γ and TNF-α were analysed by enzyme-linked immunosorbent assay. As shown in **Figure 7**, the expression level of IL-12 in each experimental group

was higher than that of the control group, and showed an upward trend with the increase of the time and frequency of medication, among which the combined treatment group had the highest level. The increase of IL-12 level should be related to the transdermal targeted delivery of *IL-12* gene to DCs. The expression of IFN-γ and TNF-α was also higher in the combined treatment group, suggesting that co-administration of the TCI patch and aPD-1 can more effectively promote the secretion of cytokines, thereby producing better anti-tumour effects.
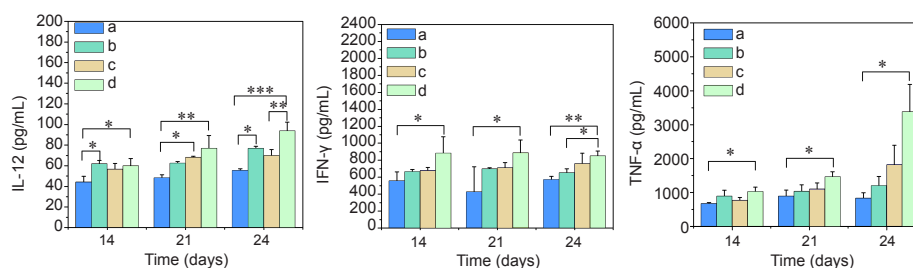

Figure 7. Expression of cytokines in the blood of melanoma-bearing mice given TCI and/or aPD-1 monotherapy treatment. a–d: Control, TCI monotherapy, aPD-1 monotherapy, and TCI + aPD-1 groups. Data are expressed as mean ± SD ($n = 3$). $*P < 0.05$, $**P < 0.01$, $***P < 0.001$ (one-way analysis of variance followed with Tukey's *post hoc* test). aPD-1: programmed cell death protein 1 monoclonal antibody; IFN-γ: interferon-γ; IL-12: interleukin-12; TCI: transcutaneous immunization; TNF-α: tumour necrosis factor-α.

Effects of different treatments on tumour growth

The tumour growth of melanoma-bearing C57BL/7 mice after different treatments is shown in **Figure 8**. The treatment of the tumor-bearing mice is shown in **Figure 8A**. Compared with the control group, different treatments showed certain inhibitory effects on tumour growth, and the combination therapy (TCI + aPD-1) group showed the most significant effect. The tumour mass of the TCI + aPD-1 group was significantly smaller than that of the aPD-1 monotherapy group, though their volumes seemed no different (**Figure 8B** & **C**). The trend of survival (**Figure 8D**) was similar to that of tumour weight (**Figure 8C**). Obviously, the anti-tumour effect of the combined treatment was significantly better than that of the monotherapy groups, indicating that TCI treatment enhanced the efficacy of aPD-1.
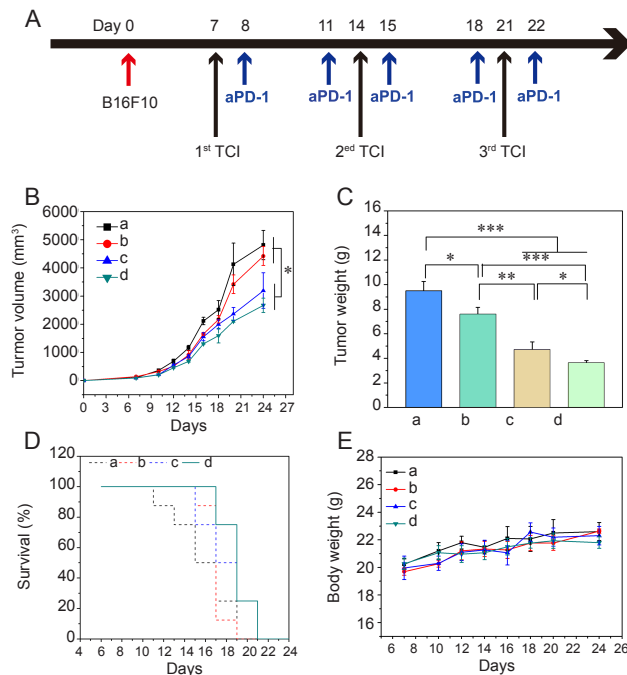
Figure 8. Schematic diagram of animal experiment protocol (A), tumour volume change curves (B), tumour weight at day 24 (C), survival rate (D) and Body weight change curves (E) in melanoma-bearing mice with TCI and/or aPD-1 treatment. a–d: Control, TCI monotherapy, aPD-1 monotherapy, and TCI + aPD-1 groups. Data are expressed as mean ± SD (n = 4). *P < 0.05, **P < 0.01, ***P < 0.001 (one-way analysis of variance followed with Tukey's *post hoc* test). aPD-1: programmed cell death protein 1 monoclonal antibody; TCI: transcutaneous immunization.

Histological analysis of the tumour tissues

To investigate the effects of different treatments on T cell recruitment and infiltration in tumour tissues, CD4 and CD8 immunohistochemical analyses were performed on tumour tissues in each group. As shown in **Figure 9A** & **B**, there were very few CD4$^+$ and CD8$^+$ T cells (showing red fluorescence) in the tumour tissues of the control group, while in the experimental groups they were more numerous. Especially, the infiltration of CD4$^+$ and CD8$^+$ T cells into the tumour tissues of the TCI + aPD-1 group was the most obvious, indicating that the transdermal targeted induction of DCs expressing IL-12 was conducive to the recruitment and infiltration of cytotoxic T cells. Terminal deoxynucleotidyl transferase dUTP nick-end labelling staining of tumour tissue stained apoptotic cells green, and the stronger the green fluorescence, the more apoptotic tumour cells were present. There were more apoptotic tumour cells in the treatment groups than in the control. The number of apoptotic tumour cells in the TCI + aPD-1 group was much greater than that in the TCI or aPD-1 monotherapy groups (**Figure 9A** & **C**). Haematoxylin–eosin staining results showed that there were more necrotic areas in the tumour tissues of each treatment group, compared with the control. Moreover, the combined treatment resulted in more necrotic areas than aPD-1 or TCI monotherapy alone. The above results indicated that transdermal delivery of the IL-12 gene targeting DCs significantly enhanced the anti-tumour effect of aPD-1 through activating cytotoxic T cells, which in turn induced apoptosis of tumour cells.

Biosafety evaluation of the combined therapy

To investigate the biosafety of the TCI patch or its combined application with aPD-1 at the *in vivo* level, the heart, liver, spleen, lung and kidney of the above experimental mice were removed, and stained with hematoxylin–eosin for histopathological analysis. As shown in **Figure 10**, there was no significant difference between the organ tissue sections of each treatment group and the control group, indicating that the TCI system used in this study has good biosafety.

Discussion

Transdermal administration has attractive development and application prospects for its advantages of avoiding first-pass effect and gastrointestinal irritation and achieving good patient compliance.[38] Needle-free TCI has also become the most promising method of immunization due to its non-invasiveness, ease of use and high efficiency.[39] In this study,
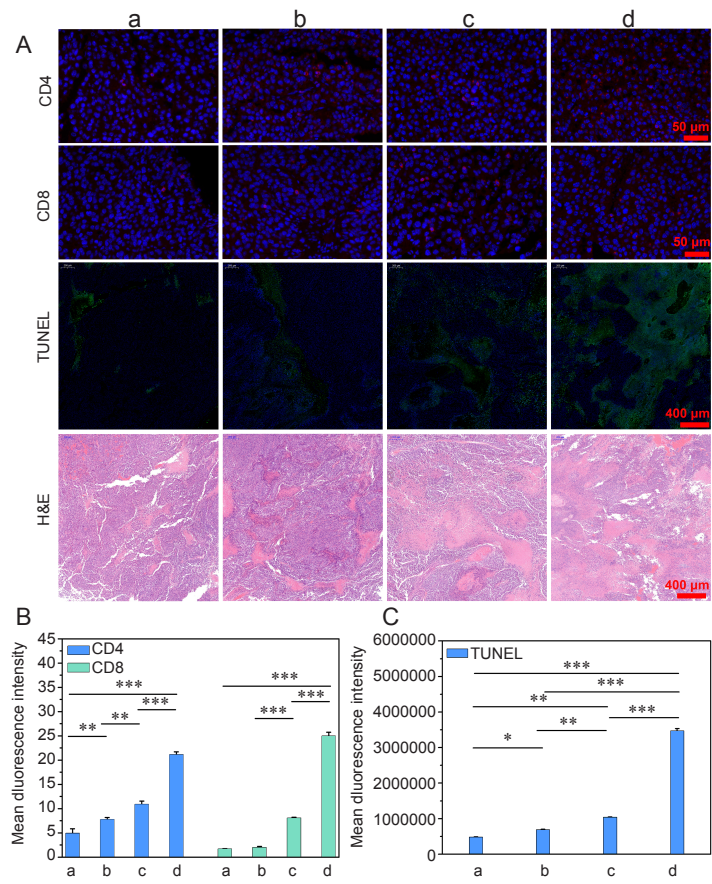
Figure 9. (A) Different staining images of tumour tissue from the melanoma-bearing mice after receiving different treatments. (B, C) Fluorescent intensity analysis of anti-CD4/CD8 or TUNEL staining. The treatment groups had more tumour cell apoptosis and more cytotoxic T cell infiltration than the control, and the combined treatment group was far better than the other groups. Scale bars: 50 and 400 μm. a-d: Control, TCI monotherapy, aPD-1 monotherapy, and TCI + aPD-1 groups. Data are expressed as mean ± SD (n = 4). *$P < 0.05$, **$P < 0.01$, ***$P < 0.001$ (one-way analysis of variance followed with Tukey's *post hoc* test). aPD-1: programmed cell death protein 1 monoclonal antibody; H&E: hematoxylin-eosin; TCI: transcutaneous immunization; TUNEL: terminal deoxynucleotidyl transferase dUTP nick-end labelling.
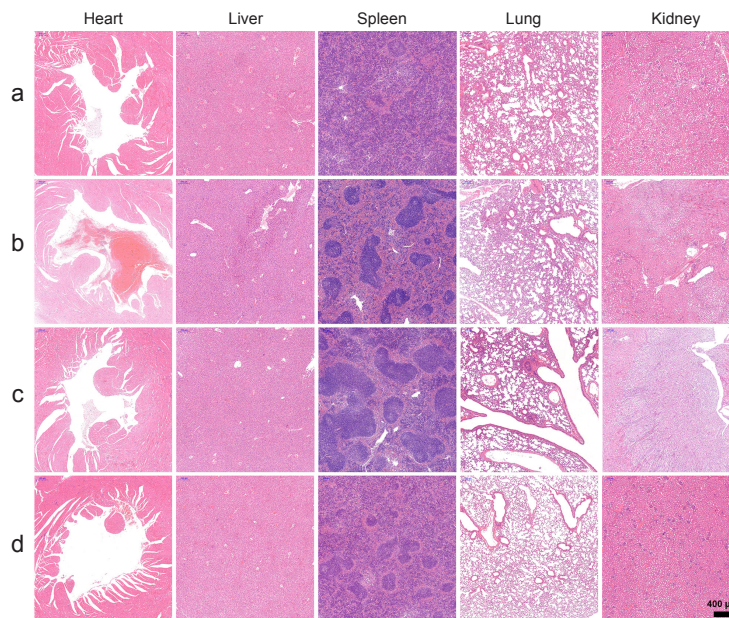

Figure 10. Histological characterization (hematoxylin–eosin staining) of the major organs from the melanoma-bearing mice after receiving different treatments. The organs showed little difference among the groups. a–d: Control, TCI monotherapy, aPD-1 monotherapy, and TCI + aPD-1 groups. Scale bar: 400 μm. aPD-1: programmed cell death protein 1 monoclonal antibody; TCI: transcutaneous immunization.

Eth[-HA] and Eth[-MC] were obtained by modifying the Eth surface with HA and MC using electrostatic adsorption and layer-by-layer self-assembly techniques. *In vitro* phagocytosis and transfection experiments showed that the Eth[-MC] possesses the ability of targeting DCs (**Figure 3**). Eth[-MC] showed a good transdermal performance, although the performance was slightly weaker than the unmodified cationic Eth (**Figure 6**), which may be due to an increase in particle size after modification. Therefore, the as-prepared Eth[-MC] can be a good TCI carrier. Flow cytometry showed that p[IL-12]@Eth[-MC] stimulate DCs to express higher levels of CD80, CD86 and major histocompatibility complex-II than p[IL-12]@Eth and lipopolysaccharide groups (**Figure 4**), indicating that p[IL-12]@Eth[-MC] effectively induce DCs to mature, which is the key to stimulating the immune response.

Due to their high specific surface area, porosity and structure similar to the natural extracellular matrix, electrospun nanofibrous mats have unique advantages for tissue regeneration and drug-controlled release.[40] Eth-loaded patches can be easily prepared by electrospinning in one step, and the obtained patches show good transdermal drug release performance.[41] However, this method has the disadvantages that the drug loading amount is limited and drug activity can be damaged in the high voltage electric field or organic solvent necessary for manufacture. In order to overcome these, electrospraying was used in this study to prepare drug-loaded microspheres and spray them onto the electrospun nanofibres. The drug loading amount could then be flexibly controlled by the electrospray time. Moreover, because the drug-loaded microspheres were sprayed onto the surface of the nanofibres, they were more likely to come into contact with cells and enter the skin tissue, compared with products prepared by one-step blend electrospinning. The drug-loaded PVP-Eth[-MC] could be easily obtained by electrospraying a mixed aqueous solution of PVP and Eth[-MC] (**Figure 5**). PVP is widely used because it has good biocompatibility and is physically inert.[24-26] In an aqueous medium, PVP can very easily dissolve and diffuse out of the matrix.[24-26] When used, the TCI patch needs to be in contact with pre-moistened skin for a closer fit. At this time, the PVP will quickly dissolve in the water, and the drug-loaded Eth[-MC] will be free to contact the skin cell membrane and fuse into the skin tissue. Here, the combination of electrospinning and electrospraying for preparation of a transdermal drug delivery patch is demonstrated to be an effective method, as the patches can effectively deliver plasmid DNA (molecular weight greater than 1×10^6) through the skin.

The antitumour effects of IL-12 have long been reported. IL-12 exerts a variety of biological effects on human T and natural killer cells *in vitro*, in addition to its ability to promote cytolytic activity, including induction of the expression of IFN-γ and other cytokines from peripheral blood T and natural killer cells.[42] However, direct injection of IL-12 protein to treat tumours in clinical practice is plagued by its short half-life, high dose demand and great safety risks.[43] The use of *IL-12* gene drugs can avoid the above drawbacks to a certain extent. Recent studies have demonstrated that the anti-tumour efficacy of aPD-1 can be significantly improved by inducing DCs to express IL-12, and the patients are less likely to suffer a relapse.[44] In this

study, we used Eth[-MC] as carriers to transdermally target DCs to deliver the *IL-12* gene. *In vitro* experiments showed that p[IL-12]@Eth[-MC] promote the expression of IL-12 by DCs, and have obvious targeting properties (**Figure 3**). Animal experiments carried out with melanoma-bearing mice as a model confirmed that applying a TCI patch of PVP-p[IL-12]@Eth[-MC]/SF-PVA to the skin significantly promoted the expression of IL-12 (**Figure 7**), and showed a certain inhibitory effect on tumour growth (**Figure 8**). When a TCI patch was co-administered with aPD-1, the expression level of IL-12 was further increased, and the levels of TNF-α and IFN-γ were also significantly increased (**Figure 7**), and showed a stronger inhibition of tumour growth than using aPD-1 alone (**Figure 8**). Further studies on the microenvironments of tumour tissues showed that apoptosis and infiltration of CD4^{+} and CD8^{+} T cells in the co-administration group were all significantly greater than in other groups (**Figure 9**), which is consistent with the data on tumour volumes and weights (**Figure 8B** & **C**). TNF-α and IFN-γ play important roles in the immune system and in monitoring tumour growth.[45] IL-12 protein generally induces the secretion of IFN-γ by cytotoxic T cells, while IFN-γ in turn has a powerful ability to stimulate DCs to express IL-12 and enhance the immune response.[46] The as-prepared TCI patch promoted the secretion of immune response-related cytokines such as IFN-γ and TNF-α by transdermal delivery of the *IL-12* gene, targeting and promoting IL-12 expression by DCs, thereby enhancing the anti-tumour effect of aPD-1 through a certain mechanism. The tissue sections of the vital organs including the heart, lung, liver, kidney and spleen showed no significant differences between the groups, indicating that the treatments with the TCI patch or/and aPD-1 which we developed have good biosafety.

In summary, co-administration of the TCI patch and aPD-1 can effectively inhibit tumour growth by enhancing the levels of IL-12, TNF-α and IFN-γ as well as promoting the infiltration of cytotoxic T cells into tumour tissues. In this study, a novel carrier, Eth[-MC], which has the performance of targeting DCs, was fabricated by modifying the mannose group on the surface of the Eth through electrostatic adsorption and layer-by-layer self-assembly methods. The p[IL-12]@Eth[-MC] were observed inducing the maturation of DCs *in vitro*. A TCI patch of PVP-p[IL-12]@Eth[-MC]/SF-PVA was obtained by electrospraying p[IL-12]@Eth[-MC]-loaded microspheres onto the surface of SF-PVA nanofibers. The TCI patches showed a good transdermal drug release performance. Applying the TCI patch to the skin of melanoma-bearing mice showed an inhibitory effect on tumour growth, and significantly enhanced the anti-tumour effect of aPD-1 without causing systemic toxicity. This approach provides a convenient and non-invasive strategy for improving the efficacy of immune checkpoint inhibitor therapy.

Conflicts of interest statement
There are no conflicts of interest to declare.
Data sharing statement

1. Tikkanen, A.; Iivanainen, S.; Koivunen, J. P. Treatment discontinuation and re-initiation of anti-PD-(L)1 agents in metastatic cancers. *J Cancer Res Clin Oncol.* **2020**, *146*, 2153-2160.

2. Aspeslagh, S.; Chabanon, R. M.; Champiat, S.; Postel-Vinay, S. Understanding genetic determinants of resistance to immune checkpoint blockers. *Semin Cancer Biol.* **2020**, *65*, 123-139.

3. Fu, J.; Kanne, D. B.; Leong, M.; Glickman, L. H.; McWhirter, S. M.; Lemmens, E.; Mechette, K.; Leong, J. J.; Lauer, P.; Liu, W.; Sivick, K. E.; Zeng, Q.; Soares, K. C.; Zheng, L.; Portnoy, D. A.; Woodward, J. J.; Pardoll, D. M.; Dubensky, T. W., Jr.; Kim, Y. STING agonist formulated cancer vaccines can cure established tumors resistant to PD-1 blockade. *Sci Transl Med.* **2015**, *7*, 283ra252.

4. Segovia, M.; Russo, S.; Jeldres, M.; Mahmoud, Y. D.; Perez, V.; Duhalde, M.; Charnet, P.; Rousset, M.; Victoria, S.; Veigas, F.; Louvet, C.; Vanhove, B.; Floto, R. A.; Anegon, I.; Cuturi, M. C.; Girotti, M. R.; Rabinovich, G. A.; Hill, M. Targeting TMEM176B enhances antitumor immunity and augments the efficacy of immune checkpoint blockers by unleashing inflammasome activation. *Cancer Cell.* **2019**, *35*,767-781.e6.

5. Nakao, S.; Arai, Y.; Tasaki, M.; Yamashita, M.; Murakami, R.; Kawase, T.; Amino, N.; Nakatake, M.; Kurosaki, H.; Mori, M.; Takeuchi, M.; Nakamura, T. Intratumoral expression of IL-7 and IL-12 using an oncolytic virus increases systemic sensitivity to immune checkpoint blockade. *Sci Transl Med.* **2020**, *12*, eaax7992.

6. Wang, M.; Liu, Y.; Cheng, Y.; Wei, Y.; Wei, X. Immune checkpoint blockade and its combination therapy with small-molecule inhibitors for cancer treatment. *Biochim Biophys Acta Rev Cancer.* **2019**, *1871*, 199-224.

7. Ruan, H.; Bu, L.; Hu, Q.; Cheng, H.; Lu, W.; Gu, Z. Strategies of combination drug delivery for immune checkpoint blockades. *Adv Healthc Mater.* **2019**, *8*, e1801099.

8. Kos, S.; Lopes, A.; Preat, V.; Cemazar, M.; Lampreht Tratar, U.; Ucakar, B.; Vanvarenberg, K.; Sersa, G.; Vandermeulen, G. Intradermal DNA vaccination combined with dual CTLA-4 and PD-1 blockade provides robust tumor immunity in murine melanoma. *PLoS One.* **2019**, *14*, e0217762.

9. Garris, C. S.; Arlauckas, S. P.; Kohler, R. H.; Trefny, M. P.; Garren, S.; Piot, C.; Engblom, C.; Pfirschke, C.; Siwicki, M.; Gungabeesoon, J.; Freeman, G. J.; Warren, S. E.; Ong, S.; Browning, E.; Twitty, C. G.; Pierce, R. H.; Le, M. H.; Algazi, A. P.; Daud, A. I.; Pai, S. I.; Zippelius, A.; Weissleder, R.; Pittet, M. J. Successful anti-PD-1 cancer immunotherapy requires T cell-dendritic cell crosstalk involving the cytokines IFN-γ and IL-12. *Immunity.* **2018**, *49*,1148-1161.e7.

10. Yao, W.; Li, Y.; Zeng, L.; Zhang, X.; Zhou, Z.; Zheng, M.; Wan, H. Intratumoral injection of dendritic cells overexpressing interleukin-12

11. Bussio, J. I.; Molina-Perea, C.; González-Aramundiz, J. V. Lower-sized chitosan nanocapsules for transcutaneous antigen delivery. *Nanomaterials (Basel).* **2018**, *8*, 659.

12. Sugita, K.; Kabashima, K.; Atarashi, K.; Shimauchi, T.; Kobayashi, M.; Tokura, Y. Innate immunity mediated by epidermal keratinocytes promotes acquired immunity involving Langerhans cells and T cells in the skin. *Clin Exp Immunol.* **2007**, *147*, 176-183.

13. Mutyambizi, K.; Berger, C. L.; Edelson, R. L. The balance between immunity and tolerance: the role of Langerhans cells. *Cell Mol Life Sci.* **2009**, *66*, 831-840.

14. Yang, X.; Wang, X.; Hong, H.; Elfawal, G.; Lin, S.; Wu, J.; Jiang, Y.; He, C.; Mo, X.; Kai, G.; Wang, H. Galactosylated chitosan-modified ethosomes combined with silk fibroin nanofibers is useful in transcutaneous immunization. *J Control Release.* **2020**, *327*, 88-99.

15. Anantaworasakul, P.; Chaiyana, W.; Michniak-Kohn, B. B.; Rungseevijitprapa, W.; Ampasavate, C. Enhanced transdermal delivery of concentrated capsaicin from chili extract-loaded lipid nanoparticles with reduced skin irritation. *Pharmaceutics.* **2020**, *12*, 463.

16. Touitou, E.; Dayan, N.; Bergelson, L.; Godin, B.; Eliaz, M. Ethosomes - novel vesicular carriers for enhanced delivery: characterization and skin penetration properties. *J Control Release.* **2000**, *65*, 403-418.

17. Mezei, M.; Gulasekharam, V. Liposomes--a selective drug delivery system for the topical route of administration. Lotion dosage form. *Life Sci.* **1980**, *26*, 1473-1477.

18. Di Blasio, S.; Wortel, I. M.; van Bladel, D. A.; de Vries, L. E.; Duiveman-de Boer, T.; Worah, K.; de Haas, N.; Buschow, S. I.; de Vries, I. J.; Figdor, C. G.; Hato, S. V. Human CD1c(+) DCs are critical cellular mediators of immune responses induced by immunogenic cell death. *Oncoimmunology.* **2016**, *5*, e1192739.

19. Unger, W. W.; van Kooyk, Y. 'Dressed for success' C-type lectin receptors for the delivery of glyco-vaccines to dendritic cells. *Curr Opin Immunol.* **2011**, *23*, 131-137.

20. Ikehara, Y.; Shiuchi, N.; Kabata-Ikehara, S.; Nakanishi, H.; Yokoyama, N.; Takagi, H.; Nagata, T.; Koide, Y.; Kuzushima, K.; Takahashi, T.; Tsujimura, K.; Kojima, N. Effective induction of anti-tumor immune responses with oligomannose-coated liposome targeting to intraperitoneal phagocytic cells. *Cancer Lett.* **2008**, *260*, 137-145.

21. Gao, H.; Gonçalves, C.; Gallego, T.; François-Heude, M.; Malard, V.; Mateo, V.; Lemoine, F.; Cendret, V.; Djedaini-Pilard, F.; Moreau, V.; Pichon, C.; Midoux, P. Comparative binding and uptake of liposomes decorated with mannose oligosaccharides by cells expressing the mannose receptor or DC-SIGN. *Carbohydr Res.* **2020**, *487*, 107877.

22. Ye, J.; Yang, Y.; Dong, W.; Gao, Y.; Meng, Y.; Wang, H.; Li, L.; Jin, J.; Ji, M.; Xia, X.; Chen, X.; Jin, Y.; Liu, Y. Drug-free mannosylated liposomes inhibit tumor growth by promoting the polarization of tumor-associated macrophages. *Int J Nanomedicine.* **2019**, *14*, 3203-3220.

23. Mata-Espinosa, D. A.; Francisco-Cruz, A.; Marquina-Castillo, B.; Barrios-Payan, J.; Ramos-Espinosa, O.; Bini, E. I.; Xing, Z.; Hernández-Pando, R. Immunotherapeutic effects of recombinant adenovirus encoding interleukin 12 in experimental pulmonary tuberculosis. *Scand J Immunol.* **2019**, *89*, e12743.

24. Luo, M.; Liang, X.; Luo, S. T.; Wei, X. W.; Liu, T.; Ren, J.; Ma, C. C.; Yang, Y. H.; Wang, B. L.; Liu, L.; Song, X. R.; He, Z. Y.; Wei, Y. Q. Folate-modified lipoplexes delivering the interleukin-12 gene for targeting colon cancer immunogene therapy. *J Biomed Nanotechnol.* **2015**, *11*, 2011-2023.

25. Takemoto, N.; Intlekofer, A. M.; Northrup, J. T.; Wherry, E. J.; Reiner,

S. L. Cutting edge: IL-12 inversely regulates T-bet and eomesodermin expression during pathogen-induced CD8+ T cell differentiation. *J Immunol.* **2006**, *177*, 7515-7519.

26. Portielje, J. E.; Lamers, C. H.; Kruit, W. H.; Sparreboom, A.; Bolhuis, R. L.; Stoter, G.; Huber, C.; Gratama, J. W. Repeated administrations of interleukin (IL)-12 are associated with persistently elevated plasma levels of IL-10 and declining IFN-gamma, tumor necrosis factor-alpha, IL-6, and IL-8 responses. *Clin Cancer Res.* **2003**, *9*, 76-83.

27. Wang, P.; Li, X.; Wang, J.; Gao, D.; Li, Y.; Li, H.; Chu, Y.; Zhang, Z.; Liu, H.; Jiang, G.; Cheng, Z.; Wang, S.; Dong, J.; Feng, B.; Chard, L. S.; Lemoine, N. R.; Wang, Y. Re-designing Interleukin-12 to enhance its safety and potential as an anti-tumor immunotherapeutic agent. *Nat Commun.* **2017**, *8*, 1395.

28. Yamasaki, S.; Sakuma, W.; Yasui, H.; Daicho, K.; Saito, T.; Fujisawa, S.; Isogai, A.; Kanamori, K. Nanocellulose xerogels with high porosities and large specific surface areas. *Front Chem.* **2019**, *7*, 316.

29. Rask, M. B.; Knopp, M. M.; Olesen, N. E.; Holm, R.; Rades, T. Influence of PVP/VA copolymer composition on drug-polymer solubility. *Eur J Pharm Sci.* **2016**, *85*, 10-17.

30. Kheradvar, S. A.; Nourmohammadi, J.; Tabesh, H.; Bagheri, B. Starch nanoparticle as a vitamin E-TPGS carrier loaded in silk fibroin-poly(vinyl alcohol)-Aloe vera nanofibrous dressing. *Colloids Surf B Biointerfaces.* **2018**, *166*, 9-16.

31. Chaubey, P.; Mishra, B. Mannose-conjugated chitosan nanoparticles loaded with rifampicin for the treatment of visceral leishmaniasis. *Carbohydr Polym.* **2014**, *101*, 1101-1108.

32. Gao, M.; Zhu, X.; Wu, L.; Qiu, L. Cationic polyphosphazene vesicles for cancer immunotherapy by efficient in vivo cytokine IL-12 plasmid delivery. *Biomacromolecules.* **2016**, *17*, 2199-2209.

33. Wang, Y.; Lin, Y. X.; Qiao, S. L.; An, H. W.; Ma, Y.; Qiao, Z. Y.; Rajapaksha, R. P.; Wang, H. Polymeric nanoparticles promote macrophage reversal from M2 to M1 phenotypes in the tumor microenvironment. *Biomaterials.* **2017**, *112*, 153-163.

34. Junyaprasert, V. B.; Boonme, P.; Wurster, D. E.; Rades, T. Aerosol OT microemulsions as carriers for transdermal delivery of hydrophobic and hydrophilic local anesthetics. *Drug Deliv.* **2008**, *15*, 323-330.

35. Chaubey, P.; Mishra, B.; Mudavath, S. L.; Patel, R. R.; Chaurasia, S.; Sundar, S.; Suvarna, V.; Monteiro, M. Mannose-conjugated curcumin-chitosan nanoparticles: Efficacy and toxicity assessments against Leishmania donovani. *Int J Biol Macromol.* **2018**, *111*, 109-120.

36. Tsepilov, R. N.; Beloded, A. V.; Samoïlenko, II. Optimization of Streptococcus equi subsp. zooepidemicus cultivation process--producer of hyaluronic acid. *Zh Mikrobiol Epidemiol Immunobiol.* **2013**, 12-20.

37. Bodade, S. S.; Shaikh, K. S.; Kamble, M. S.; Chaudhari, P. D. A study on ethosomes as mode for transdermal delivery of an antidiabetic drug. *Drug Deliv.* **2013**, *20*, 40-46.

38. Lu, J.; Guo, T.; Fan, Y.; Li, Z.; He, Z.; Yin, S.; Feng, N. Recent developments in the principles, modification and application prospects of functionalized ethosomes for topical delivery. *Curr Drug Deliv.* **2020**. doi: 10.2174/1567201817666200826093102.

39. Singh, B.; Maharjan, S.; Sindurakar, P.; Cho, K. H.; Choi, Y. J.; Cho, C. S. Needle-free immunization with chitosan-based systems. *Int J Mol Sci.* **2018**, *19*, 3639.

40. Zha, F.; Chen, W.; Zhang, L.; Yu, D. Electrospun natural polymer and its composite nanofibrous scaffolds for nerve tissue engineering. *J Biomater Sci Polym Ed.* **2020**, *31*, 519-548.

41. Laubach, J.; Joseph, M.; Brenza, T.; Gadhamshetty, V.; Sani, R. K. Exopolysaccharide and biopolymer-derived films as tools for transdermal drug delivery. *J Control Release.* **2021**, *329*, 971-987.

42. Tahara, H.; Lotze, M. T. Antitumor effects of interleukin-12 (IL-12): applications for the immunotherapy and gene therapy of cancer. *Gene Ther.* **1995**, *2*, 96-106.

43. Alsaieedi, A.; Holler, A.; Velica, P.; Bendle, G.; Stauss, H. J. Safety and efficacy of Tet-regulated IL-12 expression in cancer-specific T cells. *Oncoimmunology.* **2019**, *8*, 1542917.

44. Razi Soofiyani, S.; Kazemi, T.; Lotfipour, F.; Mohammad Hosseini, A.; Shanehbandi, D.; Hallaj-Nezhadi, S.; Baradaran, B. Gene therapy with IL-12 induced enhanced anti-tumor activity in fibrosarcoma mouse model. *Artif Cells Nanomed Biotechnol.* **2016**, *44*, 1988-1993.

45. Kobelt, D.; Zhang, C.; Clayton-Lucey, I. A.; Glauben, R.; Voss, C.; Siegmund, B.; Stein, U. Pro-inflammatory TNF-α and IFN-γ promote tumor growth and metastasis via induction of MACC1. *Front Immunol.* **2020**, *11*, 980.

46. Huang, J. H.; Zhang, S. N.; Choi, K. J.; Choi, I. K.; Kim, J. H.; Lee, M. G.; Kim, H.; Yun, C. O. Therapeutic and tumor-specific immunity induced by combination of dendritic cells and oncolytic adenovirus expressing IL-12 and 4-1BBL. *Mol Ther.* **2010**, *18*, 264-274.